H-mode access physics in MAST

P G Carolan 1), A R Field 1), H Meyer 1), C D Challis 1), G Cunningham 1), A Kirk 1), M Valovic 1), R Akers 1), E A Arends 2) P J Catto 3) N J Conway 1), G F Counsell 1), S J Fielding 1), T Fülöp 4) P Helander 1), P B Jones 5), B Lloyd 1), M McGrath 6), A Patel 1), A Sykes 1), D M A Taylor 1), M R Tournianski 1), M J Walsh 7), H R Wilson 1) and the MAST and NBI teams

1) UKAEA/EURATOM Fusion Association, Culham Science Centre, Abingdon, Oxon OX14 3DB, United Kingdom
2) FOM Institut voor Plasmafhysica Rijnhuizen, Postbus 1207, Niewwegein, Netherlands
3) Plasma Science and Fusion Centre, Massachusetts Institute of Technology, Cambridge, MA 02139, USA
4) Dept of Electromagnetics, Chalmers University of Technology, SE-412 Göteborg, Sweden
5) Imperial College of Science, Technology and Medicine, London SW7 2BZ, UK
6) University College, Dublin, Ireland
7) Walsh Scientific Ltd., Culham Science Centre, Abingdon, Oxon, OX14 3EB, UK
email patrick.carolan@ukaea.org.uk

Abstract. MAST is the first spherical tokamak (ST) reliably to deliver reproducible H-mode plasmas. Inboard gas puffing greatly facilitates the L- to H-mode transition, even in Ohmically heated plasmas. In contrast, outboard gas puffing can be exploited to inhibit H-modes, allowing detailed comparisons between otherwise near identical H- and L-mode plasmas. Connected Double Null Divertor configurations can be produced giving easier H-mode access, requiring the lowest power threshold levels for STs, only ~1.7 above the latest international power law scalings. Confinement for low frequency Type III ELM plasmas is also in agreement with the international scaling law IPB98(y,2). Recent results indicating Internal Transport Barriers are also described.

1. Introduction

The relatively low toroidal field of MAST on axis, and at the X-points, facilitates investigations at scale lengths comparable to the ion Larmor radius. In particular, the effects on H-mode transitions of inboard (i/b) and outboard (o/b) connectivity in Double Null Divertor (DND) configurations have been studied. The open geometry of MAST, with its large vessel to plasma volume ratio, provides excellent access allowing a variety of gas puffing locations and diagnostic viewing of the full plasma cross-section [1]. The smaller START experiment clearly demonstrated that L/H transitions can be obtained in STs [2, 3]. Its successor MAST provides enhanced confinement which lowers the recycling and neutral density, reducing the fast ion charge exchange loss, and providing higher temperatures (≥1keV) and lower collisionality, more typical of similarly sized conventional tokamaks. Thus transport barrier investigations in MAST allow it to play a full role in ITER relevant physics and scalings, such as ion transport, confinement, threshold powers and pedestal parameters. The large field curvature in the tight aspect ratio MAST should provide greater ITG mode stabilisation [4] and so should facilitate access to Internal Transport Barriers (ITB). Initial attempts at inducing ITBs will be described.

2. H-mode access

The first H-mode plasmas in MAST [5, 6, 7] were achieved at moderate plasma current (≤ 550 kA) and NBI heating power (≤ 0.8 MW). The resulting plasmas demonstrated all of the established H-mode signatures, including Edge Localised Modes (ELMs), increase in particle and energy confinement, steepening of the edge gradients and a sharpening of the D_α profile

at the plasma periphery. In addition, a reduction in turbulence was observed, together with a dramatic increase in the Electron Bernstein Wave (EBW) emission cone [8] and rapid acceleration of edge poloidal flow [6]. These early H-mode transitions relied for fuelling on recycling from inner graphite tiles on the central column enclosing the solenoid and toroidal field coils. Gas puffing at the i/b-midplane was incorporated [9] to provide greater H-mode control and reproducibility, allowing the limits of operating windows to be investigated such as density, current and vertical positioning. Fluxes of, typically, ~3 × 10^{21} atoms.s^{-1} are injected, allowing H-mode plasmas to be achieved reliably both with NBI and, for the first time in STs, with Ohmic heating alone [10]. Steady-state ELMy H-mode can now be maintained for periods ~200 ms at up to 1 MA plasma current with densities nearing the Greenwald limit. So far, H-modes have only been investigated in DND plasmas with typical parameters:- B_ϕ ~ 0.47 T, $I_p \leq 1.0$ MA, V_{loop} ~ 1.5 V, $q_{95} \geq 5$, R_0 ~ 0.8 m, a ~ 0.6 m, elongation ≤ 2.0 and triangularity ~ 0.45. The ELM frequency decreases with decreasing density and increasing power, as expected for Type-III ELMs. The reproducibility allows operating parameters to be optimised such as plasma shape and positioning but also shows the importance in controlling the formation phase, in particular the current density evolution. Thus, early NBI (~ 30ms) is found to delay sawteeth and internal-reconnection-events (IREs), consistent with delaying the inward diffusion of current. An abrupt reduction in the applied voltage during the discharge can also improve H-mode access and can induce ELM-free periods. This suggests that the associated reduction of edge current density increases the edge MHD stability of the plasma.

3. H-mode edge behaviour and characterisation

3.1 Effects of localised neutrals on edge rotation and electric fields

The influence of a poloidally localised neutral gas on the ion viscosity, edge plasma flow and radial electric field, and *vis-à-vis* H-mode access physics, was investigated for the first time, both experimentally and in terms of neo-classical theory [11]. Exploratory experiments on the COMPASS-D tokamak with refuelling by means of an i/b gas puff [12] were able to extend the H-mode operating window to lower densities than with puffing from the usual o/b location. Furthermore, the i/b gas puff could stimulate a transition to H-mode whereas o/b gas puffing would do the opposite, taking an H-mode back to L-mode. In MAST, i/b puffing has been used successfully to provide reliable access to sustained ELMing H-mode plasmas [9].

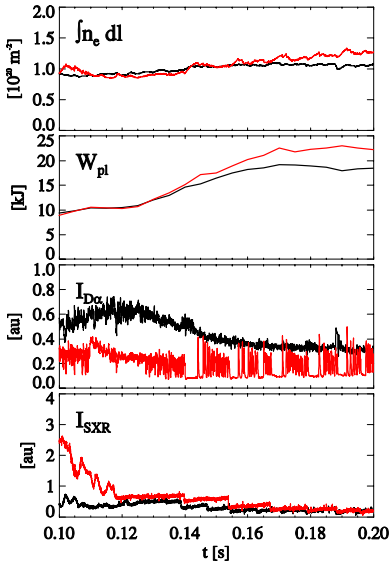

Fig. 1 Comparison of similar Ohmic discharges in MAST refuelled by inboard (#6108, red) and outboard (#6111, black) gas puffing. The D_a emission is from the upper divertor region.

Neo-classical tokamak theory has recently been extended to investigate the sensitivity of plasma flow to the poloidal localisation of the neutral density [11]. It is found that, provided the neutral fraction, n_0/n_i, exceeds 10^{-4}, the radial transport of toroidal momentum due to charge-exchange dominates that due to neo-classical viscosity and can determine the edge toroidal plasma flow and radial electric field. When the neutral density is localised poloidally, for example by a gas puff, the toroidal ion velocity, V_ϕ on a flux surface is given by:-

$$V_\phi = F_v(\theta)(R^2 B_\phi^2 / e\langle B^2 \rangle R)\, dT_i/d\psi$$

where the parameter $F_v(\theta)$ depends on the poloidal location of the gas puff, θ. The flow is in the counter-current direction for a peaked T_i profile. Larger edge outboard toroidal velocities and radial electric fields are predicted for

inboard localisation of neutrals. A possible consequent reduction of turbulent transport from velocity shear, particularly in the outboard region of poor field curvature, would facilitate the formation of an ETB [13].

Multichord Doppler spectrometry using a helium jet, developed from COMPASS-D [14], measures the He^+ ion toroidal velocity, V_ϕ, at the o/b plasma edge mid-plane. The evolution of two otherwise similar Ohmic discharges with i/b and o/b gas puffing is shown in Fig. 1 (700kA, connected-double-null-divertor, or CDND, configuration – see below -, line-average density $2\text{-}4\times10^{19}$ m^{-3}). Inboard fuelling shows a clear transition to H-mode, from dithering ELMs commencing at $t\approx0.12$s to Type-III ELMs at $t\geq0.14$s. This contrasts to the o/b fuelled discharge which remains in L-mode. Figure 2 shows the evolution of V_ϕ (measurement uncertainty, $\Delta V_\phi \approx 2$ km.s^{-1}) of He^+ ions (from the gas jet) at three values of normalised poloidal flux, ψ_N, in the region where the ETB forms. Four similar discharges are compared, with either i/b or o/b gas puff refuelling. In the gradual transition phase, with i/b gas puff, the toroidal flow increases to ≈ -10 km.s^{-1}, accompanied by enhanced flow shear, with higher velocities developing further into the plasma whereas the o/b-refuelled discharges showed little change in velocity. During each quiescent H-mode phase there is a further increase in the flow of $\Delta V_\phi \approx -5$ km.s^{-1} which is consistent with the presence of a negative (inward) radial E-field, E_r, in the ETB region.

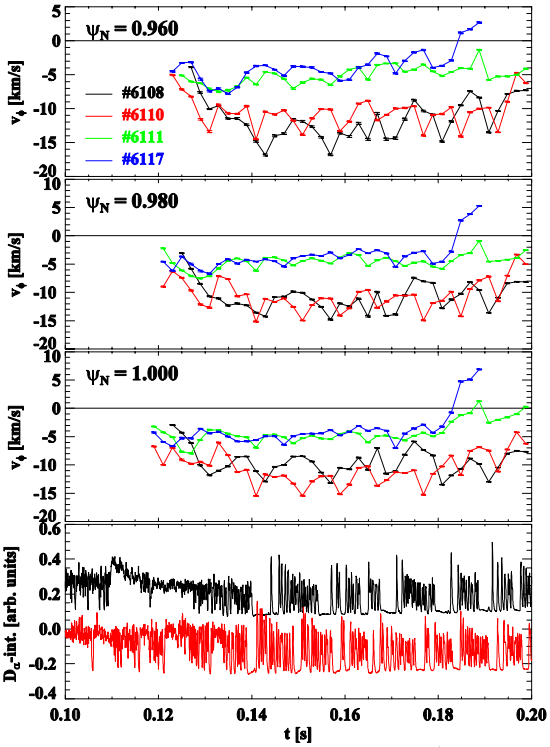

Fig. 2 The evolution of toroidal He^+ ion flow at the outer boundary of discharges with either inboard (#6108, #6110) or outboard (#6111, #6117) gas puff refuelling. Velocities are mapped onto surfaces of constant poloidal flux ψ_n.

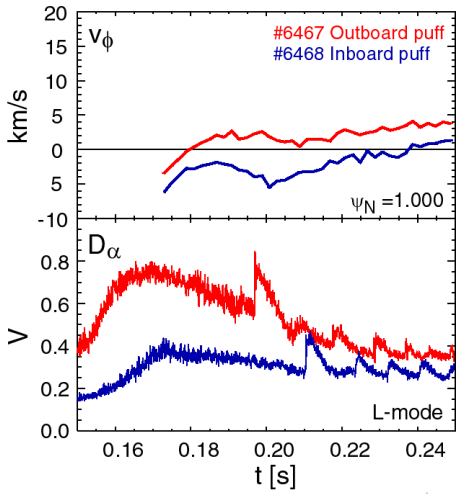

Fig. 3 The evolution of toroidal He^+ ion flow at the outer boundary of L-mode discharges with either inboard (#6468) or outboard (#6467) gas puff refuelling. Measured velocities are mapped onto surfaces of constant poloidal flux ψ_n=1

To separate effects specific to H-modes, a second series of experiments was conducted where the plasma was maintained in L-mode, by maintaining the plasma in an unconnected DND configuration (see below). As shown in Fig. 3, the toroidal flow, with i/b refuelling, differs from the o/b refuelling case by $\Delta V_\phi \approx -6$ km.s^{-1}. In these experiments the outboard edge temperature gradient, $dT_e/d\psi$, hardly changes between i/b- and o/b-refuelled discharges, *viz.* ≈ -4.5 keV Wb^{-1} r^{-1} at $\psi_{98\%}$. The observed velocity difference between discharges with i/b or o/b gas puffing is in reasonable agreement with the theoretical prediction of ≈ -9 km.s^{-1} [10]. (Note that the diagnostic monitors the He^+ ions and so the parallel velocities of the background ions may be underestimated (we estimate ~50%), because of short ionisation times from He^+ to He^{2+}.)

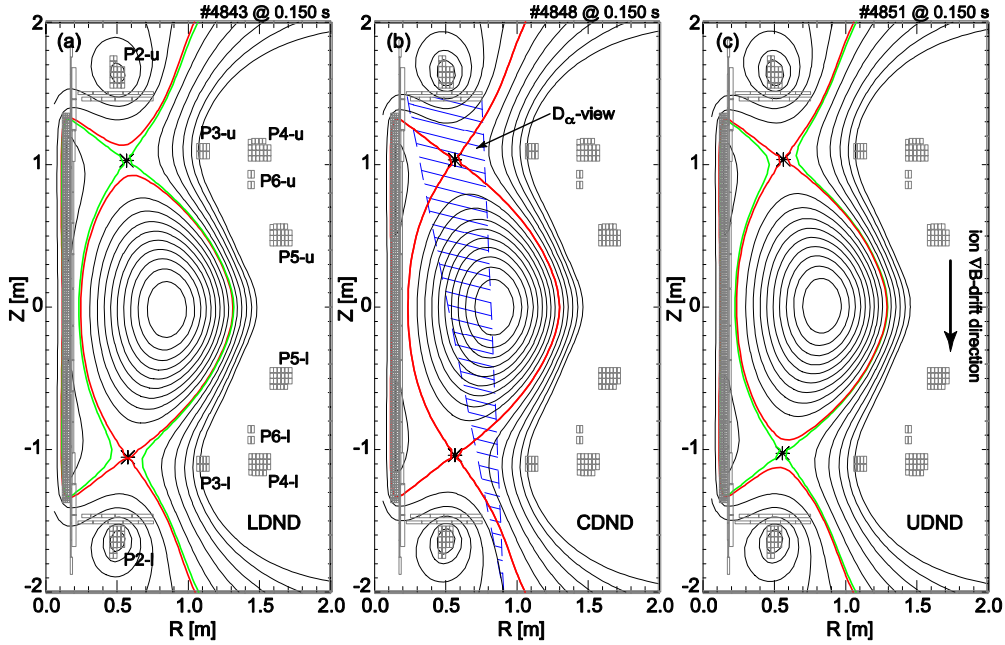

Fig. 4 EFIT reconstructions of different Double Null Divertors (DND) on MAST. (a) Lower DND, (b) Connected DND and (c) Upper DND. The red line shows the last closed flux surface (LCFS) and the green the flux surface passing through the second X-point.

3.2 Effects of close coupled separatrices in DND configurations

The influence of separatrix separation on H-mode access is investigated [15] in a set of tightly constrained Ohmic discharges, (δ=0.37 ± 0.01, κ=1.9 ± 0.05, I_p= 630 ± 30 kA, n_e = 4.0 ± 0.3 10^{19}m^{-3}, or ~40% of Greenwald density). By varying the vertical position of the magnetic axis (see Fig. 4) three distinct DNDs are achieved: lower/upper double null diverted (LDND/UDND) and connected DND (CDND) where lower/upper refers to the position of the active X-point (∇B ion drift is downwards in these experiments). A DND is regarded here as "connected" when the distance, δ_{sep}, between separatrices at the o/b mid-plane is less than the ion Larmor radius ($\rho_i \approx$ 6mm) since the cross field transport is determined at least by ρ_i and the magnetic field is lowest, and transport highest, at the o/b mid-plane. However, when the physics is better understood a more appropriate candidate may be identified for the scale length (e.g. SOL gradient length). Figure 5 shows that higher density gradients, associated with an edge transport barrier, can be sustained in connected-double-null-divertor, CDND, discharges [15] which also exhibit the usual H-mode signatures. The plasma edge density gradient is measured by the 300

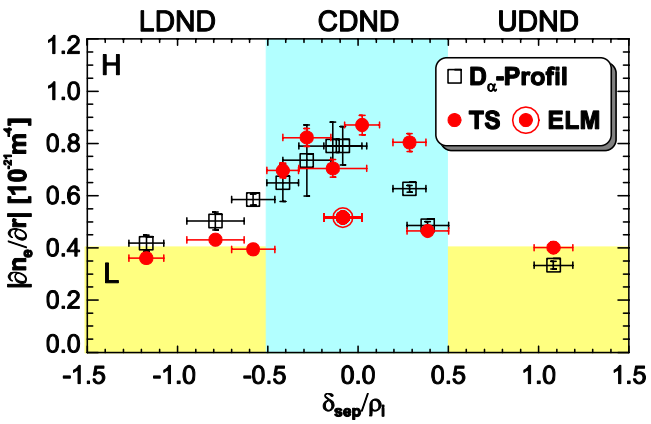

Fig. 5. Pedestal density gradient variation with normalised separatrix distance, δ_{sep}/ρ_i. Clear H-mode is achieved for connected double null divertor, CDND, when $|\delta_{sep}/\rho_i|<0.5$.

point Thomson scattering [16] and also obtained from D_α emissivity profiles [17, 18]. In contrast to the CDND, the disconnected configurations stay in L-mode. The H-mode discharges also showed higher toroidal and poloidal velocities, associated with higher radial electric fields as shown in Fig 6.

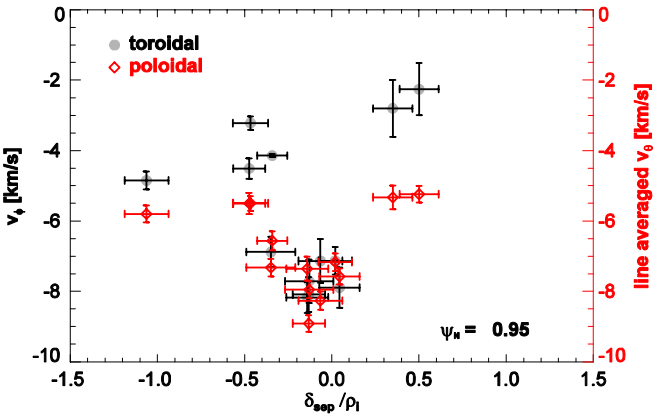

Fig. 6. Changes to the toroidal velocity, at ψ_n=0.95, and the poloidal velocity, line-of-sight emissivity weighted with normalised separatrix distance, δ_{sep}/ρ_I as in Fig. 5.The corresponding maximum radial electric field in CDND is estimated ~ -4kVm^{-1}.

The underlying physics that relates H-mode access to these different configurations, at the scale lengths comparable to ρ_i, might not be available from the usual H-mode transition models perhaps because of insufficient treatment of the effects in SOL transport. For example, the radial electric field E_r in the SOL, mainly determined by $\nabla_\perp T_e$, is expected to increase for the connected case relative to the disconnected configuration due to the differences in SOL thermal exhaust close to the LCFS [19]. This can lead to an increased electric field at the LCFS and so an enhanced electric field shear and reduced turbulence. The increased particle exhaust in the SOL in CDND may decrease the density scale length at the LCFS which may lead to reduced turbulence [20]. Indeed, in a limited series of experiments where the plasma was maintained in L-mode using o/b gas puffing, CDND discharges indicated ~40% higher edge density gradients, inside the LCFS, consistent with both descriptions.

3.3 Power threshold

MAST can make important contributions to conventional tokamak H-mode confinement and pedestal scalings primarily due to the tight aspect ratio. This is facilitated by the i/b gas refuelling allowing reproducible Connected DNDs, as described above. Thus power threshold studies for ELMy H-mode (type-III ELMs) were undertaken [21] for CDND discharges which also produce the lowest threshold powers. MAST shows a factor of ~1.7 increase in threshold power compared with a recent scaling from conventional tokamaks [22], $P_{scal}=0.061 n_{20}^{0.53} B_T^{0.78} S^{0.84}$ where n_{20} is the line average density in 10^{20}m^{-3}. Assuming that the increased threshold power in MAST is due to the inverse aspect ratio alone, this translates into a small positive dependence on the scaling threshold: $P_{scal}(\varepsilon) \propto \varepsilon^{0.5}$ [21] where $\varepsilon_{MAST} = a/R = 0.68$ whereas the central ε in the scaling database is $\varepsilon_{scal} \sim 0.26$.

3.4 Confinement

The energy confinement times in MAST ELMy H-modes are close to the $\tau_{E,scal}$ from IPB98(y,2), i.e. $\tau_{E,MAST} / \tau_{E,scal} \sim 1 \pm 0.15$. However, and perhaps more importantly, adding the MAST data to the database and removing the PBX-M data, which is at the other extreme of aspect ratios, gives an increased ε exponent of 0.80±0.05 (previously, 0.57±0.04) and an average $\langle\varepsilon\rangle \sim 0.31$ (previously, 0.29) and closer to ITER, ε_{ITER}=0.32.

3.5 Pedestals

MAST provides useful aspect ratio constraints on scalings of the edge pedestal energy as the current database uses a limited range of ε = 0.24-0.37 [23] providing no ε dependence [21].

The TS system provides greater spatial resolution on the i/b side and when combined with the greater separation of i/b flux surfaces gives unequalled resolution providing typically 10-20 points in the pedestal region. The overall diagnostic efficiency allows the pedestal parameters to be determined in a single discharge with typical results shown in Fig. 7. The measured pedestal electron energy, $W_{e,ped}$=6.8kJ, is small compared with the scaling value, *i.e.* $W_{e,ped}/W_{ped,scal}$=0.11. Making allowance for the ion energy, MAST data therefore requires a pedestal scaling that includes ε in the form: $W_{ped,scal} \propto \varepsilon^2$. MAST data are now part of International databases and for detailed analyses of the whole datasets, see [24, 25].

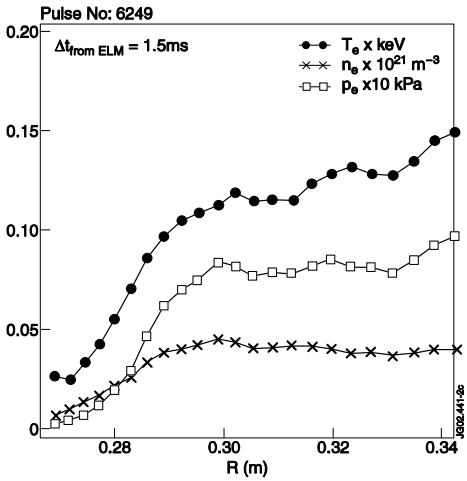

Fig 7 Edge electron temperature, density and pressure profiles from Thomson scattering.

4. Internal transport barrier access

Internal Transport Barrier (ITB) studies are important for STs, particularly for optimising the pressure gradient current drive (*e.g.* bootstrap) in a power plant [26] without a central solenoid. The relatively high field curvature may also facilitate an ITB formation by suppressing ion-thermal-gradient (ITG) modes [4]. In any case, comparisons with conventional tokamaks would extend the scaling databases and should increase understanding of both ion and electron transport in the different scenarios used in obtaining ITBs (*e.g.* velocity and magnetic shear). Preliminary experiments have been conducted to access ITBs on MAST, by applying early NBI heating and ramping up the plasma current as used on conventional tokamaks for ITB production; see Fig. 8 for a sample discharge (#7051). NBI heating (~2 MW) from two tangential beams in the co-current direction was applied from the onset, attempting to heat the plasma early and delay current penetration during the I_p ramp. By keeping the density low (n_e ~ 1x10^{19} m^{-3}) the thermal and the momentum input per particle is maximised to reduce the current diffusion and maximise the flow shear, respectively. Operating at low density allows greater beam penetration, facilitating steep internal gradients of T_e, T_i and V_ϕ.. One of the beams was in deuterium and the other in hydrogen, to enhance the CXR Doppler diagnostic. Shortly after formation of the X-points and CDND configuration (t ~ 0.07s) sheared toroidal rotation develops in the plasma core and from ~ 0.1s the stored

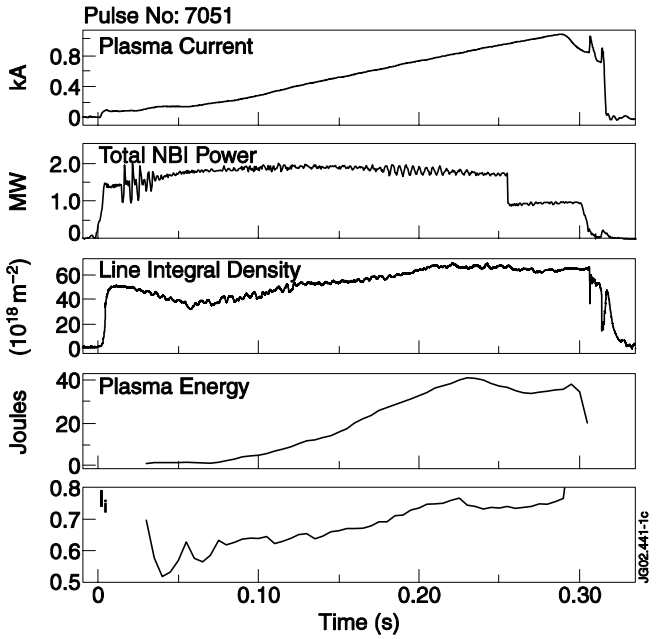

Fig. 8. Evolution of I_p, $P_{NBI,}$ $\int n_e dl$, W_{pl} and l_i from #7051.

energy, core ion temperature and SXR emission all increase indicating improved heating efficiency and ion energy confinement. Evidence for the formation of an ITB in the ion energy channel is seen at about half the minor radius where a large T_i gradient coincides with a region of high toroidal velocity shear. The C^{6+} ion temperature and velocity profiles, from CXR, are shown in Fig. 9 and the ion and electron pressure profiles in Fig. 10. (Here we assume for simplicity that the C^{6+} ions and the background ions are perfectly coupled.) The ion pressure gradient shows a marked increase in gradient where the toroidal flow shear is greatest. Even when mode activity removes the steep gradient it is observed to re-emerge as the mode decays.

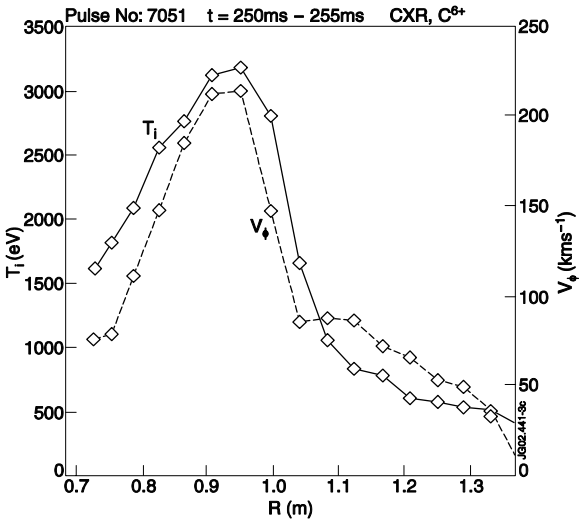

Fig 9 Ion temperature and velocity profiles from CXR for #7051

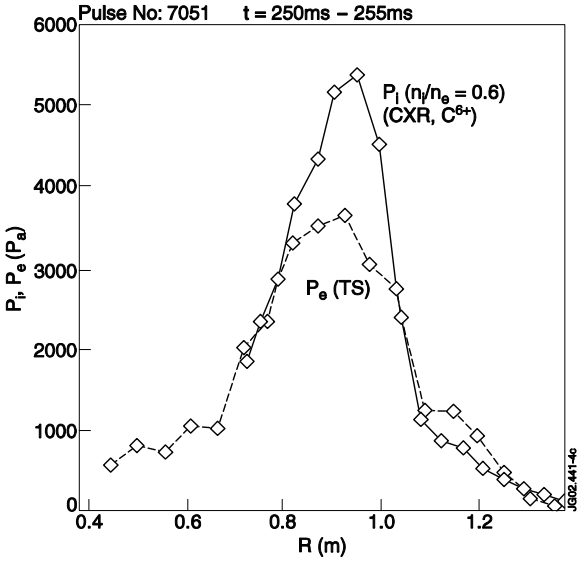

Fig 10 Ion and electron pressure profiles, for #7051, assuming an ion depletion of 0.6 consistent with the measured Zeff profile (peaked at ~3.5).

A dimensionless parameter, $\rho_T^* = \rho_s/L_T$ (ρ_s is the ion Larmor radius and L_T the temperature scale length), used to characterise the temperature gradient in conventional tokamaks, *e.g.* JET [27], gives peak values, for #7051, ρ_{Te}^* ~0.1 (at t= 160ms) and ρ_{Ti}^* ~0.2 (at t=250ms), shown in Fig. 10. Both values are above the critical values required in conventional tokamaks for ITB identification. Taking the results as a whole strongly suggests ion ITBs have been achieved in MAST but further modelling and analysis are underway, in particular to determine χ_i profiles and make comparisons with L- and H-mode plasmas.

5. Conclusions

Inboard gas puff refuelling reliably produces H-mode plasmas. Its effect on toroidal velocity has been seen that is in reasonable agreement with neo-classical predictions. Connected DND H-mode access has been investigated for the first time in tokamaks and gives the lowest threshold powers for STs. MAST contributes to the ITER relevant international databases on confinement, H-mode power threshold and pedestal energies. There is also strong evidence that Internal Transport Barriers have been achieved in MAST which is of great importance for ST power plants, and should help elucidate the physics of the ITB.

Acknowledgements
This work was jointly funded by the UK Dept. of Trade and Industry and Euratom. The NBI equipment is on loan from ORNL.

References
[1] B Lloyd *et al.*, these proceedings (Paper OV/2-3).
[2] D A Gates, R J Akers, L Appel *et al*., Phys. Plasmas **5** (5-II) 1775 (1998)
[3] P G Carolan, R J Akers, L Appel *et al*., Plasma Phys. and Contr. Fusion, **40** 615 (1998).
[4] G Rewoldt, W M Tang, S M Kaye and J Menard, Physics of Plasmas, **3** 1667 (1996).
[5] A Sykes, J-W Ahn, R J Akers *et al*., Phys. Plasmas, **8** 2101 (2001).
[6] R J Akers, G F Counsell, A Dnestrovskii *et al*., Phys. Rev. Lett. **88** 035002 (2002).
[7] R J Akers, J W Ahn, L C Appel *et al.,* Physics of Plasmas, **9** 3919 (2002).
[8] V Shevchenko *et al.,* 28th EPS Conf. on Contr. Fusion and Plasma Phys., (2001).
[9] A R Field, P G Carolan *et al*., Plasma Phys. and Contr. Fusion **44** A113 (2002).
[10] A R Field, H Meyer, A Kirk *et al*., 29th EPS Conf., Montreaux, P1.114 (2002).
[11] T Fülöp, P Helander, P J Catto, Phys. Rev. Lett., in press (2002).
[12] M Valovič, P G Carolan, A R Field *et al*, Plasma Phys. Cont. Fusion **44** A175 (2002).
[13] K H Burrell, Phys. of Plasmas **6** 12 4418 (1999).
[14] P G Carolan, N J Conway, A R Field *et al.,* Rev. Sci. Instrum., **72** 1 II 881-887 (2001).
[15] H Meyer, A Kirk, L C Appel *et al*., 29th EPS Conf., Montreaux, P1.056, (2002).
[16] M J Walsh , E R Arends, P G Carolan *et al.,* to be publ. in Rev. Sci. Instrum., (2002).
[17] M R Tournianski, P G Carolan *et al*., Nuclear Fusion **41**(1), 77 (2000).
[18] M R Tournianski, P G Carolan *et al*., to be publ. in Rev. Sci. Instrum. (2002).
[19] G F Counsell *et al*., 29th EPS Conf., Montreaux, I-1.04, (2002) to be publ. in Plasma Phys. Contr. Fusion.
[20] P Guzdar, R Kleva *et al.*, Phys. Rev. Lett. **87**(1), 15001 (2001).
[21] M Valovič, H Meyer, E R Arends *et al*., 29th EPS Conf., P1.054 (2002).
[22] F Ryter *et al*., Plasma Phys. and Contr. Fusion **44** A415 (2002).
[23] L Horton *et al*., Plasma Phys. and Contr. Fusion **44** A274 (2002).
[24] G Cordey *et al*., these proceedings (Paper CT/P-02).
[25] J Snipes *et al*., these proceedings (Paper CT/P-04).
[26] H R Wilson *et al.*, these proceedings (Paper FT/1-5).
[27] X Litaudon *et al.*, these proceedings (Paper EX/C3-4).